Dynamics of Nuclear Receptor Helix-12 Switch of Transcription Activation by Modeling Time-Resolved Fluorescence Anisotropy Decays

Mariana R. B. Batista and Leandro Martínez*
Institute of Chemistry, State University of Campinas, Campinas, SP, Brazil; and Institute of Physics of São Carlos, University of São Paulo, São Carlos, SP, Brazil

ABSTRACT   Nuclear hormone receptors (NRs) are major targets for pharmaceutical development. Many experiments demonstrate that their C-terminal Helix (H12) is more flexible in the ligand-binding domains (LBDs) without ligand, this increased mobility being correlated with transcription repression and human diseases. Crystal structures have been obtained in which the H12 is extended, suggesting the possibility of large amplitude H12 motions in solution. However, these structures were interpreted as possible crystallographic artifacts, and thus the microscopic nature of H12 movements is not well known. To bridge the gap between experiments and molecular models and provide a definitive picture of H12 motions in solution, extensive molecular dynamics simulations of the peroxisome proliferator-activated receptor-γ LBD, in which the H12 was bound to a fluorescent probe, were performed. A direct comparison of the modeled anisotropy decays to time-resolved fluorescence anisotropy experiments was obtained. It is shown that the decay rates are dependent on the interactions of the probe with the surface of the protein, and display little correlation with the flexibility of the H12. Nevertheless, for the probe to interact with the surface of the LBD, the H12 must be folded over the body of the LBD. Therefore, the molecular mobility of the H12 should preserve the globularity of the LBD, so that ligand binding and dissociation occur by diffusion through the surface of a compact receptor. These results advance the comprehension of both ligand-bound and ligand-free receptor structures in solution, and also guide the interpretation of time-resolved anisotropy decays from a molecular perspective, particularly by the use of simulations.

INTRODUCTION

Nuclear hormone receptors (NRs) are transcription regulators modulated by ligand binding. They are composed of three domains, the largest one being the ligand binding domain (LBD). The LBD is responsible for ligand recognition, but also for coactivator and corepressor binding and receptor dimerization (1,2). LBDs have a mostly preserved fold through all the NR superfamily, being composed of ~12 α-helices, which pack into a three-layer sandwich motif (3), represented in Fig. 1 A. The ligand is completely embraced by the protein in most structures that were obtained and believed to be functional (4). The burial of the ligand naturally suggests that protein conformational changes are required for ligand entry and release (5,6). Crystallographic models of the ligand-free (apo) LBDs are however, scarce, and no structure of a ligand binding intermediate is known.

The very first NR LBD structure obtained was that of the apo-LBD of the retinoic X receptor-α (RXRα) (7). The structures of the retinoic acid receptor-γ (RARγ) bound to retinoic acid and of the thyroid hormone receptor-α (TRα) bound to the natural ligand T3 followed (8,9). The most striking difference between the ligand bound (holo) and apo-structures was the position of the C-terminal Helix 12 (H12), which in the apo-RXRα structure was extended, exposing the ligand-binding pocket, but in ligand-bound RARγ and TRα were packed over the body of the LBD, completely burying the ligand (Fig. 1, A and B) (7–9).

This difference immediately suggested a mechanism for ligand entry and exit from the binding pocket in which H12 would function as a gate—this mechanism was dubbed the mouse trap model of ligand binding, and was widely accredited in the literature (10–15), including in textbooks (16). The most structurally appealing interpretation of the mouse trap model, based on the significant distension of the C-terminal H12, is probably inaccurate: The RXRα LBD crystal structure was a tetramer, with the H12 of one LBD unit laying over the coactivator groove of the other unit, a possibly nonbiological interaction (7). Furthermore, other apo-crystallographic models were obtained in which the H12 was not extended (17,18), resembling the ligand-bound models. Curiously, although the increased mobility of the H12 is associated with the ligand-free LBD, an extended-H12 ligand-bound model was obtained for the estrogen receptor (ER) (19), with a similar crystal packing artifact than the RXRα model. Therefore, although the experimental evidence supporting the existence of stable extended-H12 conformations in solution is not strong, the existence of these conformations in some crystal structures suggests that they might be relevant in solution, but unlikely to crystallize due to their increased flexibility.

Many studies have shown that the LBDs (20) and, particularly, the H12 of NRs are more flexible in the absence of ligand (21,22), but these results do not imply that this increased mobility is associated with the detachment of H12 from the body of the LBD. Structural evidence is certainly not conclusive about the extent of the H12 motions
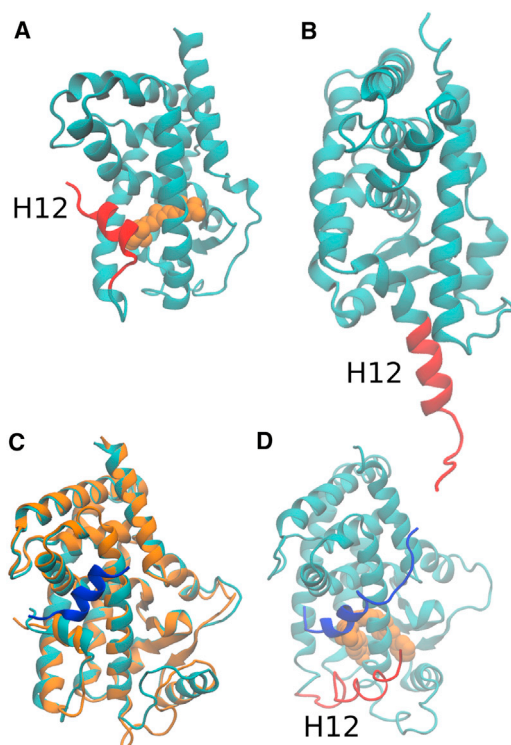
FIGURE 1   Structural diversity of H12 conformations found in crystallo-graphic models. (*A*) Crystal structure of RAR bound to all-*trans* retinoic acid (8), in which H12 traps the ligand inside the binding pocket. (*B*) Structure of apo-RXRα, displaying the extended H12 model, which suggested the mouse trap model of ligand binding (7). (*C*) Structure of PPARγ with and without ligand (17,18), which are very similar, and (*D*) structure of PPARα bound to an antagonist and a corepressor peptide (42), in which H12 is displaced from its agonist position and partially unfolded.

in peroxisome proliferator-activated receptors (PPARs): Structures of isoform PPARγ obtained without ligand (17,18), and with a ligand and a coactivator (18) are very similar, as shown in Fig. 1 *C*, although the apo-model was suggested to be a crystallographic artifact in which low affinity ligands were bound and not modeled (23), or in which crystallization was attained for the less mobile conformer, thus forcing the C-terminal helix to pack. NMR spectroscopy experiments have shown that the apo-PPARγ LBD is globally more mobile than the holo-LBD, the stabilization following the binding of strong agonists (24). The authors suggested that ligand-induced activation shifts the conformational equilibrium from a population of inactive conformers to the active form, instead of a two-state switch from an inactive to an active confor-mation. At the same time, significant displacement of the PPARα H12 is promoted by binding of a correpressor and an antagonist ligand, as shown in Fig. 1 *D* (25,26), but H12 is not extended as in apo-RXRα.

Because the dynamics of the H12 were recognized as being important for the regulation of the receptor activities, it has been studied by many experimental techniques. A notable example is the comprehensive analysis of ER

mobility by fluorescence anisotropy and fluorescence reso-nance energy transfer (27–30). Using steady-state fluores-cence anisotropy of probes attached to the LBD of ERs, Katzenellenbogen and co-workers (27) have shown that ER H12 is intrinsically dynamic, and both ligand or coacti-vator binding drive the LBD to assume a relatively rigid structure, which is resistant to proteolysis. Coactivactors can induce the LBD to assume stable forms, even in the absence of ligands (28). With fluorescence resonance energy transfer experiments, they have shown that ligand binding also stabilizes the formation and rates of dissocia-tion of dimers, which could be caused by H12 repositioning over the dimerization surface (29). Furthermore, dimeriza-tion suppressed ligand dissociation routes (29), a result to which we later provided a structural basis (31). Addition-ally, it was suggested that the lower subdomain of ER LBD can adopt a loosely folded globular state, which facil-itates ligand binding and release (30). Structural models for denaturation intermediates were suggested for TRs by our group and, in accordance with experiment, were shown to be globular (32). It is natural that modeling studies follow experimental observations, as the molecular basis for the macroscopic experimental observations can only be inferred from indirect evidence. Most of the time, however, it is not possible to directly compare the experimental results with the model data. Of course, this is due to the difficulty in obtaining experimental data on molecular motions with timescales accessible to current computer simulations.

The first molecular dynamics (MD) studies on NRs addressed the problem of ligand dissociation from RARγ (33). It was shown that H12 was likely involved in ligand dissociation, but the structures of dissociation intermediates were not consistent with the apo-RXRα structure, because the H12 did not extend. Our group has comprehensively studied ligand dissociation and binding from TRs and ERs (31,34–36). Our simulations indicate that the most favorable dissociation paths, particularly for TRs, do not involve major H12 displacements (34,35). For ERs, competing dissociation mechanisms, involving or not involving H12, were observed (31). Similar results were observed with different simulation techniques by other groups that studied ligand dissociation for other NRs (37–40). None of these simulations, with RARγ or any other NR LBD, imply the large H12 structural rearrangement suggested by the apo-RXRα structure, but it is possible to argue that the large conformational motions required for the extension of H12 were not adequately sampled in these simulations. Never-theless, we have also shown that only subtle conformational perturbations of the structure of the LBD are required even for ligand entry into the binding pocket (36). Therefore, although the simulations may not sample every possible conformation of the LBDs, they consistently suggest that major structural rearrangements as the detachment of H12 from the LBD body are, at least, not required for ligand entry or release from the binding pocket.

There is further evidence of the possible inaccuracy of extended-H12 conformations. First, many NRs actuate as transcription repressors in the absence of ligand (41) and this action is mediated by corepressor proteins that bind to the LBD. Crystallographic models of the corepressor-LBDs complexes demonstrate that corepressor peptides displace H12 from the agonist conformation, but that H12 remains packed over the LBD (42). Finally, recent Hydrogen/Deuterium-exchange experiments have shown that the H12 of TRs protects regions of the LBD in the presence or absence of ligand, thus this C-terminal helix can bind to the surface of the LBD in both cases (22). These macroscopic experiments provide hints on the equilibrium of conformations probed by H12 in solution.

A definitive analysis of the extent of H12 motions in solution requires the direct comparison of experimental data on molecular mobility with molecular models of receptor structure. In this work, we build a microscopic model of H12 motions for PPARγ. We obtain a molecular representation for the only experiment providing direct evidence on how the H12 of NRs moves with nanosecond resolution: In 2003, Schwabe and co-workers (21) performed a set of time-resolved fluorescence anisotropy decay experiments of a probe attached to the C-terminal residue of the PPARγ LBD. The time-resolved fluorescence anisotropy decay is directly correlated to the reorientational motions of the probe, most specifically to the reorientation of its transition moment vector (43,44). Once the fluorescent probe is excited by polarized light, it may emit by fluorescence at any time following excitation, and the angle of polarization of the emission of each fluorophore is related to the conformational reorientation preceding emission. Because each fluorophore reorientates differently, these movements decrease the polarization of the overall emitted light, and the rate of depolarization is dependent on how fast the probes rotate in solution. In the experiment reported by Schwabe and co-workers (21), the probe was attached to the C-terminal residue of the LBD, in such a way that the depolarization of the emission is determined by the movements of the probe relative to the C-terminal H12, the movements of the H12 (and, thus the probe) relative to the LBD and, finally, to the rotation of the whole LBD in solution (Fig. 2). Confirming previous observations, it was observed that the decay of the anisotropy was faster without ligand and faster also for LBD mutants causing human diseases (21). Therefore, they confirmed experimentally the general picture that H12 is more mobile in the absence of the ligand. Nevertheless, one more time, the analysis of the experimental data was not sufficient for the proposition of a detailed structural model of these motions.

Here, we explicitly simulate a complete model of the PPARγ LBD attached to the probe used by Schwabe and co-workers (21). The time-dependence of the anisotropy decay can be computed from the simulated motions and
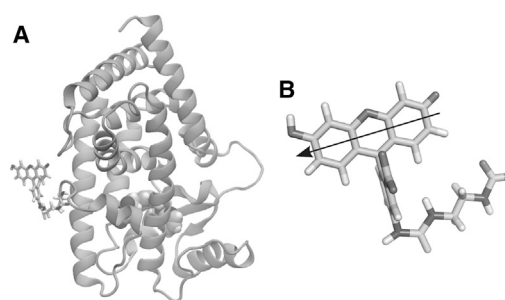

FIGURE 2 (*A*) Structural model of PPARγ bound to Rosiglitazone and attached to the CysFluor fluorescent probe. (*B*) Detail of the CysFluor probe and the orientation of its absorption dipole moment.

directly compared to the experimental results, providing a molecular level structural interpretation to their observations. We show that the observed decay rates can only be explained by the dynamics of a fluorescent probe attached to a H12, which is predominantly folded over the body of the LBD. The detachment of Helix 12 from the LBD implies much faster decay rates than the ones observed experimentally. Therefore, the LBD of PPARγ in solution (and possibly of most receptors) is compact, with packed-H12 conformations either in the presence or absence of ligand. The nature of H12 movements, which are consistent with the experimental data is shown, and its implications to the function of PPAR and other NRs are discussed.

MATERIALS AND METHODS

MD simulations were performed for PPARγ bound to Rosiglitazone and to the cysteine-fluorescein probe (CysFluor) (21), as shown in Fig. 2 *A*. CHARMM27 parameters (45) were used for the protein, and previously described CHARMM-compatible parameters (46) were used for Rosiglitazone. The parameters for CysFluor were obtained from group analogy within the CHARMM27 set, if not specified. CysFluor charges were computed using the Merz-Kollman method (47) with Gaussian03 (48) at the Hartee-Fock level using the 6-31G(d,p) basis. Three dihedral angles were parametrized for fitting the classical potential to the quantum-mechanical potential energy profile, as described in the Supporting Material, Supplementary Information 2. The parameters and simulation protocols were validated by reproducing the time-resolved fluorescence anisotropy decays of the CysFluor probe free in solution (21) (Supplementary Information 2). All parameters are available in the Supplementary Information 3. All simulations were performed with NAMD (49). VMD (50) was used for visualization and preparing figures, and the TCF module of our in-house analysis programs (51) was used for the analysis of the time correlation of the dipole moment of CysFluor in production runs (see below). The TIP3P water model was used (52). It is known that the TIP3P water model underestimates the viscosity of water (53). Therefore, we used Langevin dynamics to introduce a friction to adjust the dynamic properties of the water model to the experimental data. We first computed the self-diffusion coefficient of water in simulations of pure water with different Langevin coupling periods γ (no coupling, and γ = 1, 5, 7, and 10 ps^{-1}). With γ = 10 ps^{-1} the self-diffusion coefficient obtained from simulation (2.32 × 10^{-9} m^{2}s^{-1}) was in good agreement with the experimental value (2.30 × 10^{-9} m^{2}s^{-1}) (53,54). We then used this friction coefficient in all production runs. The same water model and correction was shown to be successful in reproducing the *cis-trans* transition kinetics of peptides bonds (55).

The time-resolved anisotropy decay was modeled from the second-order Legendre polynomial of the time-correlation function of absorption and emission dipole moments,

$$r(t) = \left(\frac{2}{5}\right) \langle P_2[\mu_a(t) \cdot \mu_e(t + \Delta t)]\rangle,$$

where μ_a and μ_e are the absorption and emission dipole moments, P_2 is the second-order Legendre polynomial operator, and $\langle\rangle$ represents the equilibrium average (44). The orientation of the absorption dipole moment vector is represented in Fig. 2 B. (44) The angles between absorption and emission dipole moments were obtained from the experimental anisotropy at $t = 0$, (44) and were 10.5° and 16.8° for holo- and apo-PPARγ, respectively. (21) The structure of PPARγ bound to Rosiglitazone (Protein Data Bank (PDB) id. 2PRG) was used. (18) The cofactor peptide was removed, and multiple initial configurations for CysFluor bound to PPARγ were obtained by running a high-temperature (800 K) simulation in vacuum in which all protein and Rosiglitazone atoms were kept fixed, for the probe to shake randomly without disturbing the protein structure. 35 aleatory configurations of the probe were extracted from this simulation and were subject to 5000 steps of conjugate-gradient (CG) energy minimization, in vacuum, also fixing all protein atoms. The energy minimized structures were solvated with Packmol (56,57) with water, sodium, and chloride ions to neutralize the simulation box. The complete systems contained ~74,000 atoms. The solvated structures were subject to the following steps of minimization and equilibration: 1), 1000 CG energy minimization and 200 ps MD keeping all protein, ligand, and probe atoms fixed. 2), 500 CG energy minimization steps and 200 ps MD keeping all Cα carbons fixed. 3), 2 ns MD. Production runs were 20 ns long and were performed from the last frame of step 3 of equilibration. All simulations were performed with a time step of 2 fs, with a constant temperature (298.15 K) and pressure (1 atm) by using a Langevin temperature bath with a damping coefficient of 10 ps^{-1} (see above) and a Langevin piston with a period of 200 fs, a decay rate of 100 fs, and a piston temperature of 298.15 K (the thermostat and barostat coupling timescales are much faster than the structural motions that determine the anistropy decay rates of this study, which are on the nanosecond timescale). A cutoff of 12 Å was used for vdW interactions with switching function starting at 10 Å. Long-range electrostatic potential were computed using the particle mesh Ewald sum method. Trajectory frames were recorded at every picosecond. Simulations following similar protocols were performed for structural models of LBDs with extended-H12 conformations. Two apo-PPARγ LBD models were built by performing steered molecular dynamics (58) (SMD) simulations starting from the holo-PPARγ LBD structure, in which H12 was pulled apart from the LBD without ligand. Two different pulling directions were used, from which two extended H12 conformations were obtained. Additionally, simulations were performed with the ER structure 1A52, (19) from which the ligand was removed, and apo-RXR (PDB id. 1LBD) (7), both experimental crystallographic models display extended-H12 conformations. The extended-H12 simulations followed the same protocol as previous runs, but only 10 random initial orientations of the probe were used for each model, extracted from high-temperature simulations. The extended-H12 mandates for a much larger simulation box, and these systems contained nearly 170,000 atoms. Finally, two auxiliary simulations of the 2PRG PPARγ model, following the same protocols, but for which production runs lasted 500 ns, were performed; one of them differing only because the Rosiglitazone molecule was removed. All simulations were run in a SGI Altix XE composed of 14 nodes with Xeon X5670 CPUs and 24 Gb of RAM memory. In summary, 65 simulations of 20 ns and 2 simulations of 500 ns were performed for solvated protein systems. The total simulation time was, therefore, 2.3 μs, excluding equilibration steps.

The fitting of the experimental curves by combinations of modeled results was performed by adjusting a linear combination of the computed curves to the experimental results in the interval of 0–5 ns. The fitting was done by implementing a constrained minimum-square fitting in which the contribution of each model curve was constrained to be between 0 and 1 and the sum of all contributions was unitary. Therefore, the parameters of the fit can be interpreted as the fractions of each model curve for the composition of the experimental data. The constrained nonlinear fit model was implemented in Fortran90 and solved with Algencan. (59) The software implementation is freely available at http://lm-utils.googlecode.com.

RESULTS AND DISCUSSION

Molecular movements and anisotropy decays in the holo-PPAR LBD

We performed MD simulations of the fluorescent probe CysFluor attached to the C-terminal residue of the ligand-bound PPARγ. Each simulation was initiated with a different conformation of the CysFluor probe, to maximize the sampling of probe conformations and possible anisotropy decay rates. Simulations were performed with the probe attached to a holo-PPARγ LBD (bound to Rosiglitazone) with H12 in agonist conformation.

The time-dependent anisotropy decay of the fluorescent probe is dependent on the reorientational dynamics of its electronic transition dipole moment. Schwabe and co-workers (21) interpreted the anisotropy decay rates by decomposing the reorientational motion of the probe into four components: 1), the probe internal structural fluctuations (not observed); 2), the movements of the probe relative to the helix (H12) to which it is attached; 3), the structural fluctuations of the H12 relative to the LBD; 4), the rotations of the LBD as a whole. The experimental time-dependent anisotropy decay combines all these movements, which occur in different timescales.

The multiple initial conformations that we used allowed for the sampling of a great diversity of reorientational movements of the probe. Each initial conformation of the probe determines a different anisotropy decay rate, and a wide variability of rates was obtained, as shown in Fig. 3. In particular, we found configurations in which the probe adheres to the protein and displays minimal motions and configurations in which the probe remains detached from the LBD during the whole simulation, displaying maximal mobility. The simulated anisotropy decay rates for holo-PPARγ display much greater variability than those observed for different experimental constructs. Specifically, when the probe remains permanently attached to the LBD (*upper gray curve* in Fig. 3), the decay rate is much slower than any of the experimentally observed rates. On the contrary, when the probe is detached from the body of the LBD (*lower curve* in Fig. 3), the simulated rate is much faster than any of the experimental results. The simulations sampled fast decay rates preferentially, because the high-temperature simulation used to model initial configurations generated conformations of the probe detached from the protein more frequently.

The experimental decays are very similar for timescales >1 or 2 ns, because of the contribution of
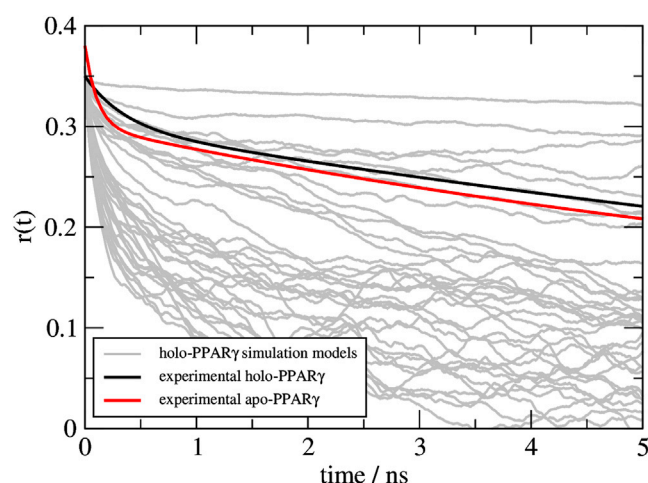
FIGURE 3 Calculated anisotropy decays for each simulation (*gray*) of holo-PPARγ, starting from different random conformations of the probe, in comparison with the experimentally observed (21) anisotropy decay rates for holo-PPARγ (*black*) and apo-PPARγ (*red*).
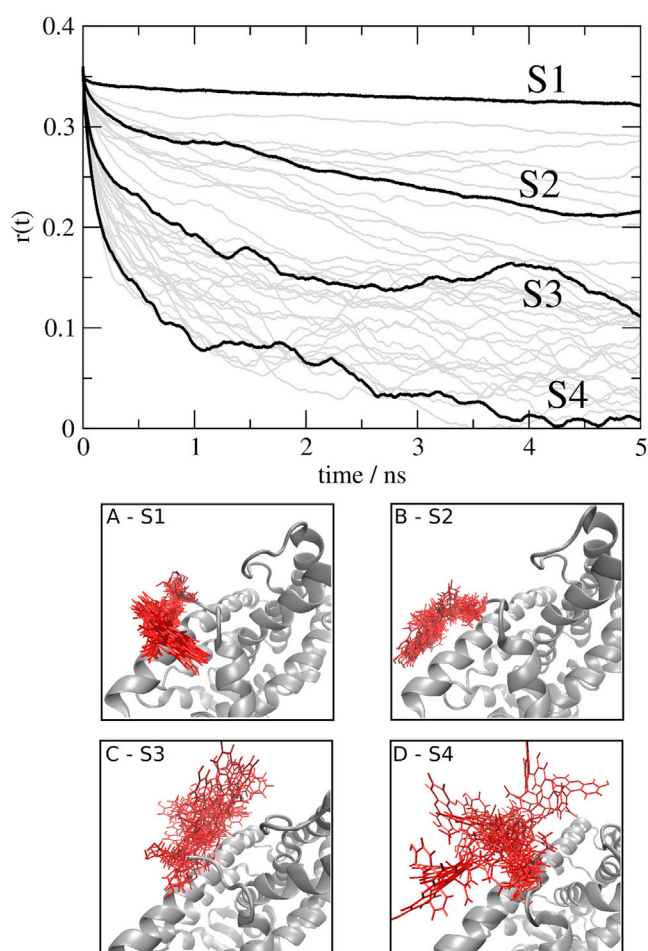

FIGURE 4 Characteristic molecular mobility of the CysFluor probe leading variable anistropy decay rates: (*A*) The slowest rate results from the docking of the probe in a cleft between H11 and H12. Intermediate decay rates result from (*B*) sliding of the probe onto the surface of the protein or (*C*) detachment from the surface in a fraction of the simulation time. (*D*) Very fast decays are characteristic of a probe that does not interact with the protein surface during the whole simulation.

reorientational motions, which are faster than protein tumbling vanish. The apo- and holo-experimental decays differ on short timescales, which are apparent before 1 ns (Fig. 3, *black* and *red*). Depending on the initial configuration, the reorientation of the probe in the simulations leads to a slow, tumbling-like decay very early in the simulations, or a full decorrelation of the anisotropy in <4 or 5 ns. Naturally, simulations displaying early tumbling-like decay are related to probe conformations that are tightly and permanently adhered to the LBD. On the other side, faster decay rates are obtained when the probe is released from the protein surface. Conformations probed by the fluorophore in representative simulations are shown in Fig. 4. The slowest decays result from the probe being attached with specific hydrogen bonds to the protein surface, restraining its mobility, as in Fig. 4 *A*. Intermediate rates are produced by conformations of the probe interacting less tightly with the protein surface, by forming only hydrophobic contacts that allow for the sliding of the probe onto the protein surface, or by the alternation of probe-attached and probe-detached configurations (Fig. 4, *B* and *C*). The fastest decay rates are observed when the protein does not interact directly with the protein surface at any time during the simulation, thus being able to randomly reorient (Fig. 4 *D*). It is important to note that these configurations presenting a probe detached from the LBD imply the full decorrelation of the probe orientation in ~5 ns (*lower black curve*, Fig. 4). The characteristic decay rates computed by triple-exponential fits are 0.014, 0.32, and 41 ns for the slowest decay, and 0.08, 0.08, and 3.31 ns for the fastest decay. Compared to experimental fits (21) to apo-PPARγ (with characteristic times of 0.08, 4.15, and 17.8 ns) and holo-PPARγ (0.35, 14.8, and 17.8 ns), we note that the slowest modeled decay displays one characteristic time (0.32 ns)

that is consistent with one characteristic time of experimental holo-PPARγ (0.35 ns), which might indicate that one experimental timescale corresponds to probe movements consistent with those of that simulation. Longer simulations (see below) would be needed for a detailed quantitative comparison of these results.

Therefore, the simulations indicate that fast decay rates are associated with large conformational motions of the probe, which occur when it does not interact with the protein surface. When these configurations predominate, decay rates are much faster than any of the experimental observations. For the tumbling-like decay to be dominant in <1 or 2 ns, the probe must be adhered to the protein surface, restricting its conformational flexibility. Therefore, the simulations show that the decay rates are determined by the propensity of the CysFluor probe to be attached to the LBD or free to rotate in solution.

Helix 12 structural fluctuations observed in Simulations S1 and S4, displaying maximal and minimal anisotropy decay rates, are shown in Fig. 5. During Simulation S1, only very minor structural fluctuations are observed, resulting in a stable and constant root mean-square deviation (RMSD) of ~1.5Å. In Simulation S4, on the other side, H12 samples two conformations, one being the crystallographic one, and a perturbed conformation, different from the crystallographic structure in ~3.5 Å RMSD. This perturbed conformation is probably induced by the high mobility of the CysFluor probe. Nevertheless, as shown in Fig. 5, the highest RMSD of H12 in this simulation is still associated with an H12, which deviates only slightly from its agonist conformation, particularly if compared, for example, with the displacements observed in the presence of a corepressor peptide (25) or with the extended-H12 model of apo-RXR (Fig. 1, B and C) (7). In every simulation, the reorientation of the H12, computed independently, is slow if compared to experimental decay rates, and essentially dominated by the global reorientation of the protein (see the Supporting Material Fig. S1), supporting the dependence of the anisotropy decay rates on the propensity of the probe to be adhered, or not, to the LBD surface. Therefore, these simulations show that there is little correlation between the anisotropy decay rates and the mobility of the protein site to which the probe is attached. Similar conclusions

were obtained for other systems, and bring to attention important limitations for the interpretation of experimental fluorescence anisotropy data. (44,60)

The holo-PPARγ simulations indicate that the time-dependence of the anisotropy of the CysFluor probe attached to H12 can span a wide range of decay rates, depending on how the probe interacts with the surface of the LBD. The experimentally observed rates would be better interpreted as a combination of local motions of a probe that partially attaches to the surface of the LBD, and partially dissociates from it. The CysFluor probe can be rigidly attached to the LBD if inserted within protein substructures (as in Simulation S1 and Fig. 4 A), or much more mobile than expected from the experiment, if detached from the body of the LBD (as in Simulation S4). Because both ligand-bound and ligand-free experimental decay rates are on the slow part of the spectrum, the probe must be able to bind to the surface of the protein in the most populated conformations in solution. We will show, now, that structural models representing the H12 in extended conformation cannot provide such a probe-protein interaction, implying that extended-H12 conformations in solution must be rare or inexistent.

How frequent can extended-H12 conformations be in PPARγ?

To evaluate the possibility of extended-H12 structures being significant for the dynamics of the LBD, we modeled the possible anisotropy decay outcomes that could result from a CysFluor probe attached to such LBD models. Because there are no experimentally available structural models of PPARγ with an extended H12, two computational constructs of PPARγ with extended-H12 were simulated, obtained from SMD simulations in which the H12 was induced to detach from the LBD. Additionally, we also performed MD simulations of the two available crystallographic extended-H12 LBD structures: the ER structure 1A52 (20) and the canonical model of apo-LBD, the apo-RXRγ (1LBD) model (7) (both might be crystallographic artifacts (7,19)). Therefore, four different structural models were used to sample the possible interactions of the CysFluor probe with apo-LBDs, and determine whether experimentally observed decay rates could be interpreted as the decay rates resulting from the reorientational dynamics of the probe attached to these extended-H12 structures. The models are represented in Fig. 6, A–C.

The predicted time-resolved fluorescence decays for the open-H12 models are displayed in Fig. 6. The decay is much faster than that observed for most closed-H12 models, resembling, on average, the fastest decay of those models. The probe cannot form contacts to the core of the protein, and fluctuates without major steric impairment, resulting in fast reorientational dynamics. In all cases, the decay rates are significantly faster than any of the experimental measures for apo, holo, and mutant PPARγ LBDs. (21)
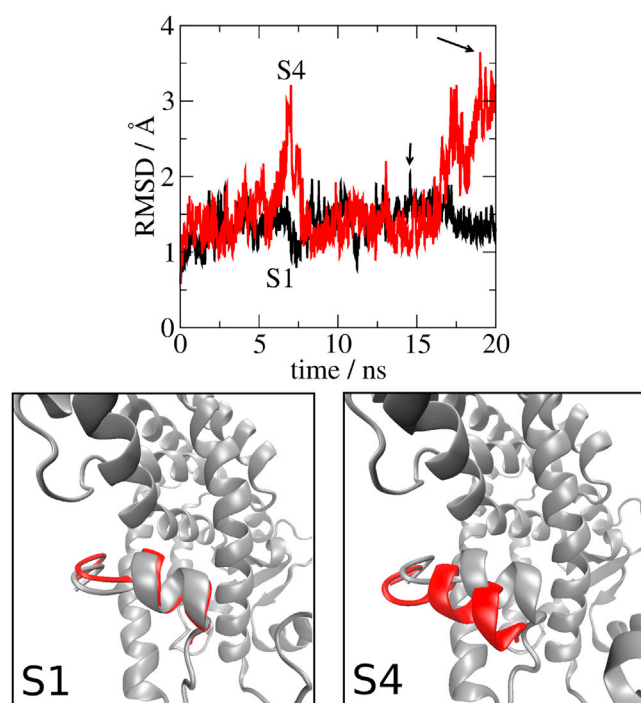

FIGURE 5 Mobility of the H12 of PPARγ LBD in simulations displaying extreme decay rates (see Fig. 4). The maximum displacement in each simulation is indicated and shown. Simulation S1 displays the slowest decay rate and is related to minor H12 displacements. Simulation S4 displays a decay rate much faster than experimental ones, and greater but still subtle H12 movements.
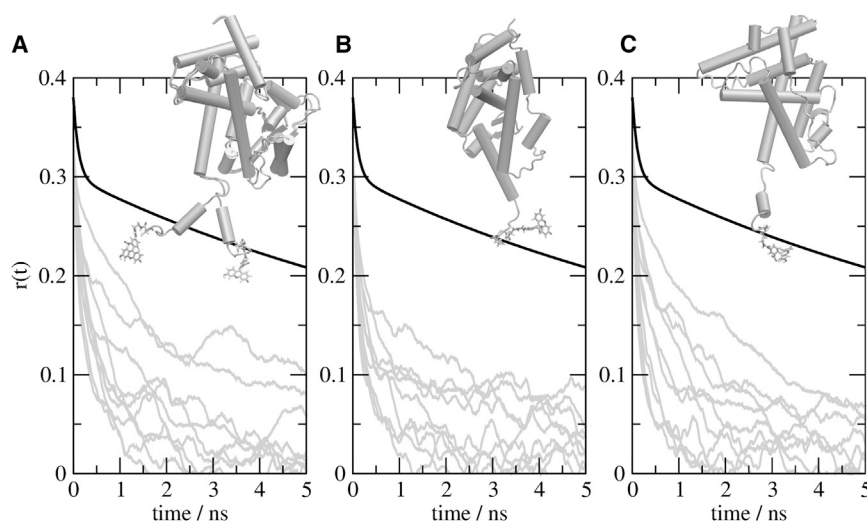
FIGURE 6 Extended-H12 models simulated and the computed time-resolved anisotropy responses. The black lines represent the experimental apo-PPARγ decay ([21]), and gray lines are simulated curves. All simulated curves decay much faster than the experimental result, for all models, because the probe cannot interact with the protein surface. (*A*) PPARγ models obtained from SMD simulations (two superimposed models are shown). (*B*) The apo-RXRα crystallographic structure ([7]). (*C*) The extended-H12 ER crystallographic structure ([19]).

Therefore, the experimentally observed anisotropy decays, if having at all a contribution from extended-H12 structures, must be compensated by the prevalence of structures in which the probe lays down over the body of the LBD. We will first try to reproduce the experimental curves from single long simulations of compact LBDs, and then compute quantitatively the frequency distribution of the different simulated decays that best fit the experimentally obtained rates.

Modeling anisotropy decays from long simulations of a globular PPARγ

Ideally, a single simulation would be able to sample all possible conformations of the probe and of the receptor in such a way that the anisotropy decays computed would reproduce the experimental results. Therefore, in view of the fact that our previous results indicated that extended-H12 models appeared not to be necessary for obtaining the experimental decays, we performed relatively long simulations of the PPARγ LBD starting from one of the conformations used in the previous simulations. Two 500 ns simulations were performed starting from the same model, the Rosiglitazone ligand removed from one of the structures. Therefore, these simulations should provide insights into the dynamics of apo- and holo-LBDs, whenever the structure remains compact in both cases.

The mobilities of the CysFluor probe observed in each simulation are shown in Fig. 7. The simulations started with conformation of the probe detached from the LBD, in such a way that the probe displays a high conformational variability until the instant in which it lays down over the surface of the LBD. The instants of attachment of the probe to the protein surface are very clear, resulting in small fluctuations of the RMSD in subsets of the simulations. Although the initial structures are identical, the mobilities of the probe differ. In the ligand-bound simulation

(Fig. 7 *A*), the probe was observed to fluctuate until ~200 ns, when it assumed a relatively rigid conformation by interacting with the protein surface. No major conformational changes were observed in the remaining 300 ns of simulation.

On the other side, the probe in the ligand-free model oscillated until ~100 ns, when it reached a less mobile state by interacting with the protein surface. However, different from what was observed with ligand, this conformation was not stable. The probe deviates progressively from this initial surface-bound state, dissociates from the surface at ~300 ns, and until the end of the simulation, transitions between different conformations occurred ~5 times (indicated by arrows). Therefore, the probe was indeed more mobile in the ligand-free model. Each conformation of the probe persisted for 20 to 100 ns, indicating that for the proper sampling of this conformational variability one would need simulations of several microseconds. The same estimate cannot be done for the ligand-bound simulations, as no interchange between conformations was observed (therefore, the required simulations might be much longer). Fig. 7, *E* and *F*, represent the mobility of the CysFluor probe and of H12 in these long simulations. A superposition of snapshots representative of the mobilities after 200 ns is shown. The conformational variability of H12 in both simulations is similar, and the conformational variability of the probe is slightly larger in the ligand-free simulation, reflecting the conformational shifts of the probe indicated in Fig. 7 *B*. For each simulation, the probe persistently interacted with the same region of the LBD after laying down over the surface of the protein.

With the limited sampling provided by these simulations in mind, we nevertheless computed the anisotropy decays that the mobilities of the probes imply (Fig. 7, *C* and *D*). The decay of the ligand-bound anisotropy agrees reasonably with the experimental result in short timescales (Fig. 7 *C*). The higher mobility of the probe in the ligand-free
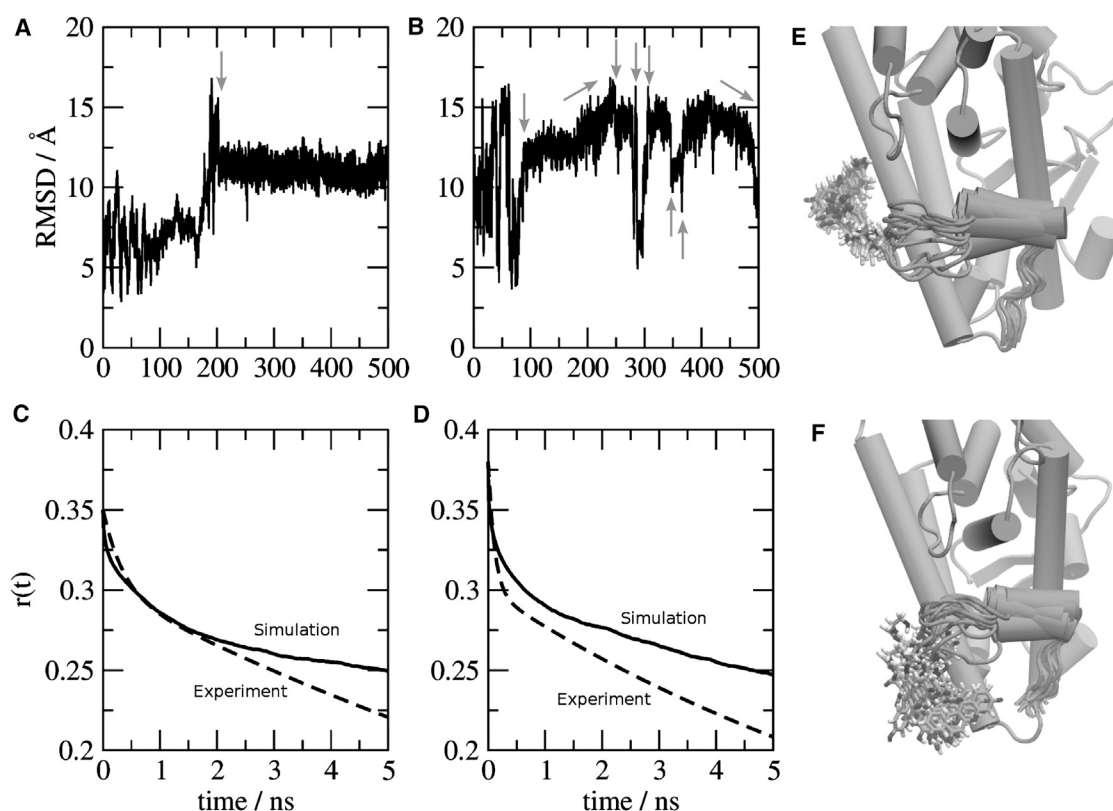
FIGURE 7   Mobility and anisotropy decays in 500 ns-long simulations. (*A*) RMSD of the CysFluor probe in ligand-bound (holo) PPARγ. (*B*) RMSD of the CysFluor probe in ligand-free PPARγ. Time-resolved anisotropy decays computed from the 500 ns simulations for (*C*) holo-PPARγ and (*D*) ligand-free PPARγ. Solid lines represent the decays computed from the computational models and dashed lines the experimental observation (21). Molecular representation of the movements experienced by the CysFluor probe and the H12 in the last 300 ns of these simulations for (*E*) ligand free PPARγ and (*F*) holo-PPARγ.

simulation also roughly reproduces the experimental apo-PPARγ decay (Fig. 7 *F*). Both simulations underestimate the rate of the tumbling of the protein, and deviate from the experimental result at longer timescales (this might result from the Langevin dynamics, some protein diffusivity limitation due to the size of the simulation box, or simply lack of sampling, as some variability of tumbling rates was obtained for the shorter MD simulations, as shown in Fig. S1).

## Experimental decays as weighted combinations of simulation models

We cannot precisely reproduce in a single simulation the experimental decay rates because transitions between dynamic states that lead to different anisotropy responses are too rare to be sampled effectively. Therefore, we have implemented a constrained least-square fitting approach, (59) and obtained the best linear combination of the model curves that reproduce the experimental observations, in each case. The coefficients of the fit can be interpreted as the fractional contribution of each model curve to the experimental decay (or, equivalently, the percentage of the time in which the probe displays a particular configuration in solution).

This strategy is justified by the 500 ns simulations, which show that the probe conformations persist much longer than the timescales of interest (0 to 5 ns), and in such a way that the experimental result can be considered a weighted combination of the possible depolarization outcomes.

In Fig. 8 *A*, we show the reconstruction of the experimental holo-PPARγ curve as a combination of the simulated holo-PPARγ decays. A very good fit can be obtained, as noted by the overlap of the experimental and reconstructed curves (*black* and *red*). The optimal combination of simulated decays that fit the experimental observation is composed by an approximate fifty-fifty combination of models that display decays slower than the experimental ones and models that display decays faster than the experimental ones (this is not an obligatory result: if, for example, the faster decays were slower than actually computed, their total contribution would have to be larger than ~50% to compensate for the slower decays).

Experimentally, the apo-PPARγ decay is faster than the holo-PPARγ decay on short timescales. However, the experimental apo-PPARγ decay cannot be reproduced using only extended-H12 models (Fig. 8 *B*), as is evident from the fact that all these models displayed decay rates faster than the
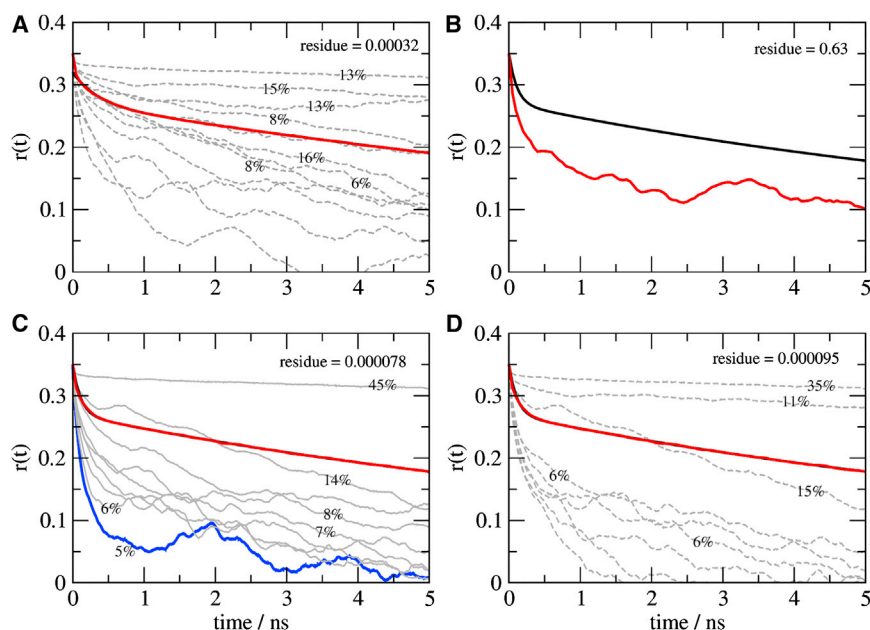
FIGURE 8 Contributions of each model for reproducing the experimental decays. Curves with contributions >2% are shown, and contributions >5% are labeled. The red curve is the best least-square fitting to the experimental data, which is depicted in black (in *panels A*, *C*, and *D*, the *black* and *red curves* almost overlap). (*A*) Optimal fitting of the holo-PPARγ experimental decay using all simulations of holo-PPARγ LBD. (*B*) Fitting of experimental apo-PPARγ decay fails using extended-H12 models, because no model produces decay slower than the experimental one, the best fit is simply the reproduction of the simulated curve with the slowest decay (*red*). The experimental apo-PPARγ decay can be nicely fit if considering holo-PPARγ models, with (*C*) a minor contribution of extended-H12 models (*blue*), or (*D*) without extended-H12 models at all.

experimental ones. This indicates that one needs significant contributions of probe conformations attached to the LBD body to interpret the experimental observation also for apo-PPARγ. In Fig. 8 *C*, we computed the combination of all simulated curves (both from holo-PPARγ models and extended-H12 PPAR models) that best reproduce the experimental apo-PPARγ decay. Now it is possible to reproduce with great precision the experimental curve, which requires, as predicted, a great contribution of probe conformations attached to LBD—particularly the 45% contribution of the slowest decay rate observed. The greatest contribution to this fit coming from extended-H12 models is 5% (*blue curve* in Fig. 8 *C*), suggesting that extended-H12 configurations might not be required at all for the interpretation of the experimental result. Indeed, as Fig. 8 *D* indicates, the fitting of the experimental apo-PPARγ decay using only the closed-H12 holo-PPARγ models is also precise. The fast decay rates are adequately reproduced by closed-H12 models in which the probe is detached from the body of the LBD, and the slow experimental decay at intermediate timescales is granted by the tightly bound probes in slow-decay models.

Therefore, the experimental decay rates can be reproduced if there is a significant contribution of conformations of the probe, which are tightly attached to the LBD surface, displaying slow-decay rates. Faster decay rates result not from the detachment of the H12 from the body of the LBD, but from the detachment of the probe from the LBD body. The need of 50% contribution of configurations in which the probe is able to lay over the LBD surface is, we believe, a strong argument against the existence, to any significant extent, of extended-H12 structures in solution. In particular, if the extended-H12 configurations were significantly populated, the experimental decays would

imply the great predominance of CysFluor-H12 interaction-specific attachments in every closed-H12 conformation. We cannot rule out this possibility but it is, at least, unlikely.

We suggest, therefore, that H12 must be folded over the LBD in solution with or without ligand, and also if subject to the particular mutations studied by Schwabe and co-workers. (21) If existent at all, extended-H12 conformations must be very poorly populated and most likely do not have any role in ligand binding and dissociation, or corepressor recruitment. Ligand or cofactor binding must stabilize the position of H12 in agonist or antagonist conformations in a structural equilibrium that occurs in a receptor that remains compact, although less rigid, without ligand. The NMR spectroscopy experiments reported by Johnson et al. (24) are particularly consistent with this view: as they demonstrate that the LBD of apo-PPARγ is as a whole more mobile and possibly structurally diverse, it is natural that the probe would be less tightly attached to its surface, although the receptor may preserve its globularity in every conformation. This model of LBD motions is also consistent with the minor displacements required for ligand entry and release previously discussed on the basis of MD simulations on TRs (34,35) and other receptors (33,37,38), and also with H/D exchange experiments on TRs that suggest the protection of H3 by H12 in the ligand-free receptor. (22)

CONCLUSIONS

Nanosecond-resolution fluorescence anisotropy experiments are one of the few experiments providing dynamic data that can be directly compared to molecular movements with atomic resolution obtained by simulations. With

improved computer power, software, and methods, MD simulations have recently reached the timescales necessary for the qualitative comparison of modeled anisotropy decay rates with experimental data on fluorescent probes attached to relatively large proteins. (44,60) Here, we compare the results from MD simulations directly to experimental data on NR LBD movements, providing limiting bounds to the range of motions of the C-terminal H12 of PPARγ.

In this work, we show that the molecular movements of a fluorescent probe attached to the Helix 12 are consistent with experimental anisotropy decays and correspond to local fluctuations not involving the detachment of this helix from the LBD. The detachment of the fluorescent probe from the body of the LBD results in anisotropy decays, which are much faster than any of the experimental observations reported. Therefore, the conformations of H12 in solution must permit the interaction of the probe with the surface of the LBD, implying that the H12 cannot be extended. This implies that ligand entry and release, and cofactor binding or dissociation, impose structural fluctuations to H12 that preserve the globularity of the structure. The picture of a persistently compact LBD is consistent with many previous experimental and simulation results.

The present results advance the comprehension of the range of motions that H12 may undergo in solution both in the presence or absence of ligands. We reinforce the interpretation of extended-H12 models as crystallographic artifacts and, thus, suggest that the mouse trap model of ligand binding, as originally proposed, is most likely imprecise. We do not rule out the possibility that H12 is involved in ligand binding and dissociation to some receptors, but its movements should be local if the range of mobilities of the H12 observed here for PPARγ are representative. On the other side, we must attend to the possibility that the LBD of other receptors, particularly RXR, may display different conformational equilibria. This study provides the basis for the interpretation of time-resolved fluorescence anisotropy experiments on other LBDs, as the anisotropy decays resulting from extended-H12 models are qualitatively different from those resulting from compact LBDs.

More generally, our results confirm the possibility of lack of correlation of the reorientational dynamics of the probe and of the protein site to which it is bound. Fluorescence anisotropy experiments must be interpreted with care, because the experimental anisotropies might not correspond directly to changes in the mobility of the site to which the probe is attached. (44,60) We show that one of the mechanisms for this lack of correlation might be the dissociation of the fluorophore from the protein surface.

SUPPORTING MATERIAL

Five figures and supporting information are available at http://www.biophysj.org/biophysj/supplemental/S0006-3495(13)00850-3.

REFERENCES

1. Kumar, R., and E. B. Thompson. 1999. The structure of the nuclear hormone receptors. *Steroids.* 64:310–319.

2. Darimont, B. D., R. L. Wagner, …, K. R. Yamamoto. 1998. Structure and specificity of nuclear receptor-coactivator interactions. *Genes Dev.* 12:3343–3356.

3. Bourguet, W., P. Germain, and H. Gronemeyer. 2000. Nuclear receptor ligand-binding domains: three-dimensional structures, molecular interactions and pharmacological implications. *Trends Pharmacol. Sci.* 21:381–388.

4. Weatherman, R. V., R. J. Fletterick, and T. S. Scanlan. 1999. Nuclear-receptor ligands and ligand-binding domains. *Annu. Rev. Biochem.* 68:559–581.

5. Wurtz, J. M., W. Bourguet, …, H. Gronemeyer. 1996. A canonical structure for the ligand-binding domain of nuclear receptors. *Nat. Struct. Biol.* 3:87–94.

6. Klaholz, B. P., and D. Moras. 1998. A structural view of ligand binding to the retinoid receptors. *Pure Appl. Chem.* 70:41–47.

7. Bourguet, W., M. Ruff, …, D. Moras. 1995. Crystal structure of the ligand-binding domain of the human nuclear receptor RXR-alpha. *Nature.* 375:377–382.

8. Renaud, J. P., N. Rochel, …, D. Moras. 1995. Crystal structure of the RAR-gamma ligand-binding domain bound to all-trans retinoic acid. *Nature.* 378:681–689.

9. Wagner, R. L., J. W. Apriletti, …, R. J. Fletterick. 1995. A structural role for hormone in the thyroid hormone receptor. *Nature.* 378:690–697.

10. Germain, P., L. Altucci, …, H. Gronemeyer. 2003. Nuclear receptor superfamily: Principles of signaling. *Pure Appl. Chem.* 75:1619–1664.

11. Moras, D., and H. Gronemeyer. 1998. The nuclear receptor ligand-binding domain: structure and function. *Curr. Opin. Cell Biol.* 10:384–391.

12. Nettles, K. W., and G. L. Greene. 2005. Ligand control of coregulator recruitment to nuclear receptors. *Annu. Rev. Physiol.* 67:309–333.

13. Yen, P. M. 2001. Physiological and molecular basis of thyroid hormone action. *Physiol. Rev.* 81:1097–1142.

14. Desvergne, B., and W. Wahli. 1999. Peroxisome proliferator-activated receptors: nuclear control of metabolism. *Endocr. Rev.* 20:649–688.

15. Comba, A., Y. H. Lin, …, M. E. Pasqualini. 2011. Basic aspects of tumor cell fatty acid-regulated signaling and transcription factors. *Cancer Metastasis Rev.* 30:325–342.

16. Krauss, G. 2003. Biochemistry of Signal Transduction and Regulation, 3rd ed. Wiley-VCH, Weinheim, Germany.

17. Uppenberg, J., C. Svensson, …, A. Berkenstam. 1998. Crystal structure of the ligand binding domain of the human nuclear receptor PPAR-gamma. *J. Biol. Chem.* 273:31108–31112.

18. Nolte, R. T., G. B. Wisely, …, M. V. Milburn. 1998. Ligand binding and co-activator assembly of the peroxisome proliferator-activated receptor-gamma. *Nature.* 395:137–143.

19. Tanenbaum, D. M., Y. Wang, …, P. B. Sigler. 1998. Crystallographic comparison of the estrogen and progesterone receptor's ligand binding domains. *Proc. Natl. Acad. Sci. USA.* 95:5998–6003.

20. Pissios, P., I. Tzameli, …, D. D. Moore. 2000. Dynamic stabilization of nuclear receptor ligand binding domains by hormone or corepressor binding. *Mol. Cell.* 6:245–253.

21. Kallenberger, B. C., J. D. Love, ..., J. W. Schwabe. 2003. A dynamic mechanism of nuclear receptor activation and its perturbation in a human disease. *Nat. Struct. Biol.* 10:136–140.

22. Figueira, A. C., D. M. Saidemberg, ..., I. Polikarpov. 2011. Analysis of agonist and antagonist effects on thyroid hormone receptor conformation by hydrogen/deuterium exchange. *Mol. Endocrinol.* 25:15–31.

23. Liberato, M. V., A. S. Nascimento, ..., I. Polikarpov. 2012. Medium chain fatty acids are selective peroxisome proliferator activated receptor (PPAR) γ activators and pan-PPAR partial agonists. *PLoS ONE.* 7:e36297.

24. Johnson, B. A., E. M. Wilson, ..., G. Zhou. 2000. Ligand-induced stabilization of PPARgamma monitored by NMR spectroscopy: implications for nuclear receptor activation. *J. Mol. Biol.* 298:187–194.

25. Xu, H. E., T. B. Stanley, ..., J. B. Stimmel. 2002. Structural basis for antagonist-mediated recruitment of nuclear co-repressors by PPARalpha. *Nature.* 415:813–817.

26. Nagy, L., and J. W. Schwabe. 2004. Mechanism of the nuclear receptor molecular switch. *Trends Biochem. Sci.* 29:317–324.

27. Tamrazi, A., K. E. Carlson, and J. A. Katzenellenbogen. 2003. Molecular sensors of estrogen receptor conformations and dynamics. *Mol. Endocrinol.* 17:2593–2602.

28. Tamrazi, A., K. E. Carlson, ..., J. A. Katzenellenbogen. 2005. Coactivator proteins as determinants of estrogen receptor structure and function: spectroscopic evidence for a novel coactivator-stabilized receptor conformation. *Mol. Endocrinol.* 19:1516–1528.

29. Tamrazi, A., K. E. Carlson, ..., J. A. Katzenellenbogen. 2002. Estrogen receptor dimerization: ligand binding regulates dimer affinity and dimer dissociation rate. *Mol. Endocrinol.* 16:2706–2719.

30. Gee, A. C., and J. A. Katzenellenbogen. 2001. Probing conformational changes in the estrogen receptor: evidence for a partially unfolded intermediate facilitating ligand binding and release. *Mol. Endocrinol.* 15:421–428.

31. Sonoda, M. T., L. Martínez, ..., I. Polikarpov. 2008. Ligand dissociation from estrogen receptor is mediated by receptor dimerization: evidence from molecular dynamics simulations. *Mol. Endocrinol.* 22:1565–1578.

32. Martínez, L., P. C. T. Souza, ..., M. S. Skaf. 2010. On the denaturation mechanisms of the ligand binding domain of thyroid hormone receptors. *J. Phys. Chem. B.* 114:1529–1540.

33. Blondel, A., J. P. Renaud, ..., M. Karplus. 1999. Retinoic acid receptor: a simulation analysis of retinoic acid binding and the resulting conformational changes. *J. Mol. Biol.* 291:101–115.

34. Martínez, L., M. T. Sonoda, ..., I. Polikarpov. 2005. Molecular dynamics simulations reveal multiple pathways of ligand dissociation from thyroid hormone receptors. *Biophys. J.* 89:2011–2023.

35. Martínez, L., P. Webb, ..., M. S. Skaf. 2006. Molecular dynamics simulations of ligand dissociation from thyroid hormone receptors: evidence of the likeliest escape pathway and its implications for the design of novel ligands. *J. Med. Chem.* 49:23–26.

36. Martínez, L., I. Polikarpov, and M. S. Skaf. 2008. Only subtle protein conformational adaptations are required for ligand binding to thyroid hormone receptors: simulations using a novel multipoint steered molecular dynamics approach. *J. Phys. Chem. B.* 112:10741–10751.

37. Carlsson, P., S. Burendahl, and L. Nilsson. 2006. Unbinding of retinoic acid from the retinoic acid receptor by random expulsion molecular dynamics. *Biophys. J.* 91:3151–3161.

38. Kosztin, D., S. Izrailev, and K. Schulten. 1999. Unbinding of retinoic acid from its receptor studied by steered molecular dynamics. *Biophys. J.* 76:188–197.

39. Peräkylä, M. 2009. Ligand unbinding pathways from the vitamin D receptor studied by molecular dynamics simulations. *Eur. Biophys. J.* 38:185–198.

40. Shen, J., W. Li, ..., H. Jiang. 2009. Computational insights into the mechanism of ligand unbinding and selectivity of estrogen receptors. *J. Phys. Chem. B.* 113:10436–10444.

41. Hörlein, A. J., A. M. Näär, T. Heinzel, J. Torchia, B. Gloss, R. Kurokawa, A. Ryan, Y. Kamei, M. Söderström, C. K. Glass..., 1995. Ligand-independent repression by the thyroid hormone receptor mediated by a nuclear receptor co-repressor. *Nature.* 377:397–404.

42. Watson, P. J., L. Fairall, and J. W. R. Schwabe. 2012. Nuclear hormone receptor co-repressors: structure and function. *Mol. Cell. Endocrinol.* 348:440–449.

43. Cross, A. J., and G. R. Fleming. 1984. Analysis of time-resolved fluorescence anisotropy decays. *Biophys. J.* 46:45–56.

44. Schröder, G. F., U. Alexiev, and H. Grubmüller. 2005. Simulation of fluorescence anisotropy experiments: probing protein dynamics. *Biophys. J.* 89:3757–3770.

45. MacKerell, A. D., D. Bashford, M. Bellott, R. L. Dunbrack, J. D. Evanseck, M. J. Field..., 1998. All-atom empirical potencial for molecular modeling and dynamics studies of proteins. *J. Phys. Chem. B.* 102:3586–3616.

46. Hansson, A., P. C. T. Souza, ..., M. S. Skaf. 2009. Charmm force field parametrization of roziglitazone. *Int. J. Quantum Chem.* 111: 1346–1354.

47. Singh, U. C., and P. A. Kollman. 1984. An approach to computing electrostatic charges for molecules. *J. Comput. Chem.* 5:129–145.

48. Frisch, M. J., G. W. Trucks, ..., J. A. Pope. 2004. Gaussian 03, revision C.02. Gaussian, Wallingford, CT.

49. Phillips, J. C., R. Braun, ..., K. Schulten. 2005. Scalable molecular dynamics with NAMD. *J. Comput. Chem.* 26:1781–1802.

50. Humphrey, W., A. Dalke, and K. Schulten. 1996. VMD: visual molecular dynamics. *J. Mol. Graph.* 14:33–38, 27–28.

51. Martínez, L. 2013. LM-MDanalysis, version 13.060. Campinas.

52. Jorgensen, W. L., J. Chandrasekhar, ..., M. L. Klein. 1983. Comparison of simple potencial functions for simulating liquid water. *J. Chem. Phys.* 79:926–935.

53. Mark, P., and L. Nilsson. 2001. Structure and dynamics of the TIP3P, SPC and SPC/E water models at 298K. *J. Phys. Chem.* 105:9954–9960.

54. Mills, R. 1973. Self-diffusion in normal and heavy water in the range 1–45°. *J. Phys. Chem.* 77:685–688.

55. Doshi, U., and D. Hamelberg. 2011. Extracting realistic kinetics of rare activated processes from accelerated molecular dynamics using Kramers' theory. *J. Chem. Theory Comput.* 7:575–581.

56. Martínez, J. M., and L. Martínez. 2003. Packing optimization for automated generation of complex system's initial configurations for molecular dynamics and docking. *J. Comput. Chem.* 24:819–825.

57. Martínez, L., R. Andrade, ..., J. M. Martínez. 2009. PACKMOL: a package for building initial configurations for molecular dynamics simulations. *J. Comput. Chem.* 30:2157–2164.

58. Isralewitz, B., M. Gao, and K. Schulten. 2001. Steered molecular dynamics and mechanical functions of proteins. *Curr. Opin. Struct. Biol.* 11:224–230.

59. Andreani, R., E. G. Birgin, ..., M. L. Schuverdt. 2007. On augmented Lagrangian methods with lower-level constraints. *SIAM J. Optim.* 18:1286–1309.

60. Scott, D. R., C. F. Vardeman, 2nd, ..., B. M. Baker. 2012. Limitations of time-resolved fluorescence suggested by molecular simulations: assessing the dynamics of T cell receptor binding loops. *Biophys. J.* 103:2532–2540.